PROCEEDINGS OF SCIENCE

# *CP* violation in multi-body charmless *b*-hadron decays at LHCb

**Adam Morris***
*Aix Marseille Univ, CNRS/IN2P3, CPPM, Marseille, France*
*E-mail:* adam.morris@cern.ch

Long-distance resonant dynamics along with a sizeable weak phase present in multi-body charmless *b*-hadron decays leads to rich structures of *CP* violation as a function of the phase space. Amplitude analysis provides a deeper understanding of the mechanisms that generate strong phase variations, which are responsible for this effect. We present the amplitude analyses of $B^+ \to \pi^+K^+K^-$ and $B_s^0 \to K_S^0K^\pm\pi^\mp$ decays. For the former, *CP* asymmetries of the contributing quasi-two-body resonances are measured. Charmless *b*-baryon decays represent a promising opportunity to make a first observation of *CP* violation in the baryonic sector. We also present the most recent measurements of four-body charmless *b*-baryon decays performed by LHCb.

*European Physical Society Conference on High Energy Physics - EPS-HEP2019 -*
*10-17 July, 2019*
*Ghent, Belgium*

*Speaker.





PoS(EPS-HEP2019)215

## 1. Introduction

Direct *CP* violation requires amplitudes with differences in both their weak and strong phases. Charmless $b$-hadron decays can proceed simultaneously via tree-level $b \to u$ and loop-level $b \to s$ or $b \to d$ transitions, which gives rise to a sizeable weak phase difference. The resonant structures of multi-body $b$-hadron decays can give rise to large strong-phase differences, which can lead to enhanced *CP* violation in certain regions of phase space.

Amplitude analysis is necessary to understand the resonant structures of multi-body decays and to measure the variation of relative strong phases over the phase space. Multi-body charmless $b$-baryon decays also show potential for making a first observation of *CP* violation in baryons. In these proceedings, three measurements of *CP* violation in multi-body $b$-hadron decays are presented. All three use proton-proton collision data collected by the LHCb detector corresponding to $3\,\text{fb}^{-1}$ of integrated luminosity at $\sqrt{s} = 7$ and 8 TeV.

## 2. Amplitude analysis of $B_s^0 \to K_S^0 K^\pm \pi^\mp$ decays

The branching fraction of the decay $B_s^0 \to K_S^0 K^\pm \pi^\mp$ and its quasi-two-body decays ($K^{*\pm} K^\mp$ and $K^{*0} K_S^0$) have been previously measured by LHCb [1, 2, 3, 4]. A full untagged and time-integrated amplitude analysis, published in Ref. [5], is presented in these proceedings. The dataset is split into $K_S^0 K^+ \pi^-$ and $K_S^0 K^- \pi^+$ final states, and the signal regions for the amplitude analysis are defined as $\pm 2.5\sigma$ around the nominal value of the $B_s^0$ mass, where $\sigma$ is the mass resolution determined by a fit to the $K_S^0 K^\pm \pi^\mp$ invariant mass distributions, shown in Figure 1. There are 431.1 $\overline{(}B\overline{)}_s^0 \to K_S^0 K^+ \pi^-$ candidates and 489.9 $\overline{(}B\overline{)}_s^0 \to K_S^0 K^- \pi^+$ candidates in the defined signal regions.

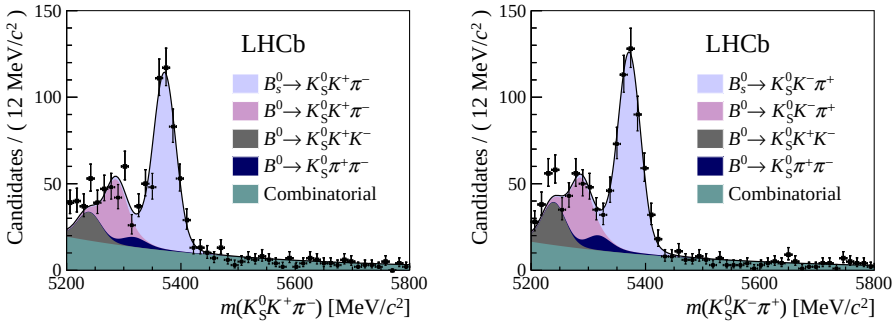


**Figure 1:** Invariant mass distributions of candidates in the data for the (left) $K_S^0 K^+ \pi^-$ and (right) $K_S^0 K^- \pi^+$ final states.

Both $B_s^0$ and $\bar{B}_s^0$ mesons can decay to each final state, although not necessarily with the same amplitude, *i.e.* $A_f \neq \overline{A}_f$. The lack of flavour tagging means that the $B_s^0$ and $\bar{B}_s^0$ contributions cannot be distinguished. A simultaneous amplitude fit is performed to both final states to extract an effective amplitude that is a combination of $A_f$ and $\overline{A}_f$. Resonances decaying to $K^+ K_S^0$, *e.g.* the $a_2(1320)^+$ are considered but not seen in the fit. The $K_S^0 \pi^\mp$ and $K^\pm \pi^\mp$ P-wave and D-wave resonances are modelled with relativistic Breit–Wigner lineshapes and include the $K^*(892)$ and $K_2^*(1430)$ states. The $K_S^0 \pi^\mp$ and $K^\pm \pi^\mp$ S-wave components are modelled with the LASS parametrisation [6], which combines the $K_0^*(1430)$ and non-resonant $K\pi$ components, but in a way that makes it possible to disentangle the $K_0^*(1430)$ when calculating fit fractions.

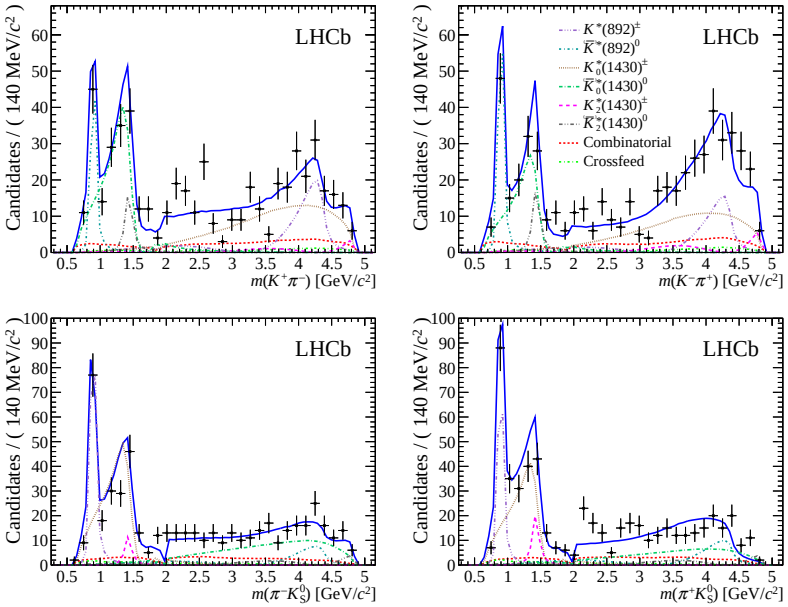


**Figure 2:** Projections onto $m(K^\pm\pi^\mp)$ (top) and $m(\pi^\mp K^0_S)$ (bottom) of the amplitude fit to the $K^0_S K^+\pi^-$ (left) and $K^0_S K^-\pi^+$ (right) final states.

| $K^0_S K^+\pi^-$ | | $K^0_S K^-\pi^+$ | |
|---|---|---|---|
| Contribution | Frac. (%) | Contribution | Frac. (%) |
| $K^*(892)^-$ | $15.6\pm1.5\pm\ 6.3$ | $K^*(892)^+$ | $13.4\pm2.0\pm\ 1.8$ |
| $K_0^*(1430)^-$ | $30.2\pm2.6\pm22.3$ | $K_0^*(1430)^+$ | $28.5\pm3.6\pm15.2$ |
| $K_2^*(1430)^-$ | $2.9\pm1.3\pm\ 2.9$ | $K_2^*(1430)^+$ | $5.8\pm1.9\pm\ 6.9$ |
| $K^*(892)^0$ | $13.2\pm2.4\pm\ 7.4$ | $\bar{K}^*(892)^0$ | $19.2\pm2.3\pm\ 8.5$ |
| $K_0^*(1430)^0$ | $33.9\pm2.9\pm\ 5.7$ | $\bar{K}_0^*(1430)^0$ | $27.0\pm4.1\pm\ 6.8$ |
| $K_2^*(1430)^0$ | $5.9\pm4.0\pm\ 6.0$ | $\bar{K}_2^*(1430)^0$ | $7.7\pm2.8\pm\ 6.3$ |

**Table 1:** Fit fractions extracted from the $B^0_s\to K^0_S K^\pm\pi^\mp$ amplitude fit. The first uncertainties are statistical and the second systematic.

Projections of the fitted amplitude model onto the $K^\pm\pi^\mp$ and $\pi^\mp K^0_S$ invariant mass distributions are shown in Figure 2. The fit fractions for each resonance are given in Table 1. Each resonance and its conjugate have a consistent fit fraction, thus no significant *CP* violation is observed. Systematic uncertainties arise from the mismodelling of the mass fit, variation of the efficiency and background models, fit biases, uncertainties on fixed parameters and variations of the amplitude model.

The flavour-averaged fit fractions from the amplitude analysis are converted to branching fractions of quasi-two-body decays:

$$\begin{aligned}
\mathscr{B}(B^0_s\to K^*(892)^\pm K^\mp) &= (18.6\pm1.2\pm0.8\pm\ 4.0\pm2.0)\times10^{-6},\\
\mathscr{B}(B^0_s\to K_0^*(1430)^\pm K^\mp) &= (31.3\pm2.3\pm0.7\pm25.1\pm3.3)\times10^{-6},\\
\mathscr{B}(B^0_s\to K_2^*(1430)^\pm K^\mp) &= (10.3\pm2.5\pm1.1\pm16.3\pm1.1)\times10^{-6},
\end{aligned}$$

$$\begin{aligned}
\mathscr{B}(B_s^0 \to \overline{(}K^*(892)^0\overline{)}^0) &= (19.8 \pm 2.8 \pm 1.2 \pm \ \ 4.4 \pm 2.1) \times 10^{-6}, \\
\mathscr{B}(B_s^0 \to \overline{(}K_0^*(1430)^0\overline{)}^0) &= (33.0 \pm 2.5 \pm 0.9 \pm \ \ 9.1 \pm 3.5) \times 10^{-6}, \\
\mathscr{B}(B_s^0 \to \overline{(}K_2^*(1430)^0\overline{)}^0) &= (16.8 \pm 4.5 \pm 1.7 \pm 21.2 \pm 1.8) \times 10^{-6}.
\end{aligned}$$

The uncertainties, in order, are statistical, systematic, due to the choice of model and due to the uncertainty on the total $B_s^0 \to K_S^0 K^\pm \pi^\mp$ branching fraction [2]. These results represent the first observation of the $B_s^0 \to K_0^*(1430)^\pm K^\mp$ and $B_s^0 \to \overline{(}K_0^*(1430)^0\overline{)}^0$ decay modes.

Additionally, the branching fractions of the non-resonant modes are determined to be

$$\begin{aligned}
\mathscr{B}(B_s^0 \to (\overline{(}K^0\overline{)}\pi^\pm)_{\rm NR} K^\mp) &= (11.4 \pm 0.8 \pm 0.2 \pm 9.2 \pm 1.2 \pm 0.5) \times 10^{-6}, \\
\mathscr{B}(B_s^0 \to (K^\mp \pi^\pm)_{\rm NR}\, \overline{(}K^0\overline{)}) &= (12.1 \pm 0.9 \pm 0.3 \pm 3.3 \pm 1.3 \pm 0.5) \times 10^{-6},
\end{aligned}$$

where the fifth uncertainty is related to proportion of the $(K\pi)_0^*$ component due to the effective range part of the LASS lineshape.

## 3. Amplitude analysis of $B^\pm \to \pi^\pm K^+ K^-$ decays

*CP* asymmetries in the decay $B^\pm \to \pi^\pm h^+ h'^-$ have previously been measured by LHCb using a binned model-independent analysis [7]. The total *CP* asymmetry in $B^\pm \to \pi^\pm K^+ K^-$ was measured to be

$$\mathscr{A}^{CP} \equiv \frac{\Gamma(B^- \to f^-) - \Gamma(B^+ \to f^+)}{\Gamma(B^- \to f^-) + \Gamma(B^+ \to f^+)} = -0.123 \pm 0.017 \pm 0.012 \pm 0.007,$$

where the uncertainties are statistical, systematic and due to the uncertainty in the *CP* asymmetry of the $B^\pm \to J/\psi K^\pm$ reference mode. A sizeable local *CP* asymmetry was observed in the region of $\pi^+\pi^- \leftrightarrow K^+K^-$ rescattering. This warrants an amplitude analysis to investigate further.

An amplitude analysis of $B^\pm \to \pi^\pm K^+ K^-$ decays is published in Ref. [8] and presented in these proceedings. The dataset is split into $\pi^+ K^+ K^-$ and $\pi^- K^+ K^-$ final states, and the signal regions for the amplitude analysis are defined as $5.266 < m(\pi^\pm K^+ K^-) < 5.300\,\text{GeV}/c^2$. A simultaneous fit to $m(\pi^\pm K^+ K^-)$ in both samples yields $2052 \pm 102$ $B^+ \to \pi^+ K^+ K^-$ and $1566 \pm 84$ $B^- \to \pi^- K^+ K^-$ candidates.

Resonances decaying to the $\pi^\pm K^\mp$ and $K^+K^-$ final states are modelled with relativistic Breit–Wigner lineshapes. The non-resonant $\pi^\pm K^\mp$ contribution is described by a single-pole form-factor, proposed in Ref. [9]

$$\mathscr{A}_{\rm source} = \left(1 + \frac{s}{\Lambda^2}\right)^{-1}, \tag{3.1}$$

where $s = m^2(\pi^\pm K^\mp)$ and $\Lambda$ (chosen to be $1\,\text{GeV}/c^2$) sets the scale for the energy dependence. The $\pi^+\pi^- \leftrightarrow K^+K^-$ rescattering amplitude is described using

$$\mathscr{A}_{\rm rescattering} = \left(1 + \frac{s}{\Lambda^2}\right)^{-1} \sqrt{1-\nu^2}\, e^{2i\delta}, \tag{3.2}$$

where $s = m^2(K^+K^-)$ and the inelasticity, $\nu$, and phase shift, $\delta$, are parametrised as in Ref. [10]

$$\nu = 1 - \left(\varepsilon_1 \frac{k_2}{\sqrt{s}} + \varepsilon_2 \frac{k_2^2}{s}\right) \frac{M'^2 - s}{s}, \tag{3.3}$$

$$\cot\delta = C_0 \frac{(s - M_s^2)(M_f^2 - s)}{M_f^2 \sqrt{s}} \frac{|k_2|}{k_2^2}, \tag{3.4}$$

where $k_2 = \frac{1}{2}\sqrt{2-4m_K^2}$, $m_K = 0.495\,\text{GeV}/c^2$, $M' = 1.5\,\text{GeV}/c^2$, $M_s = 0.92\,\text{GeV}/c^2$, $M_f = 1.32\,\text{GeV}/c^2$, $\varepsilon_1 = 2.4$, $\varepsilon_2 = -5.5$ and $C_0 = 1.3$.

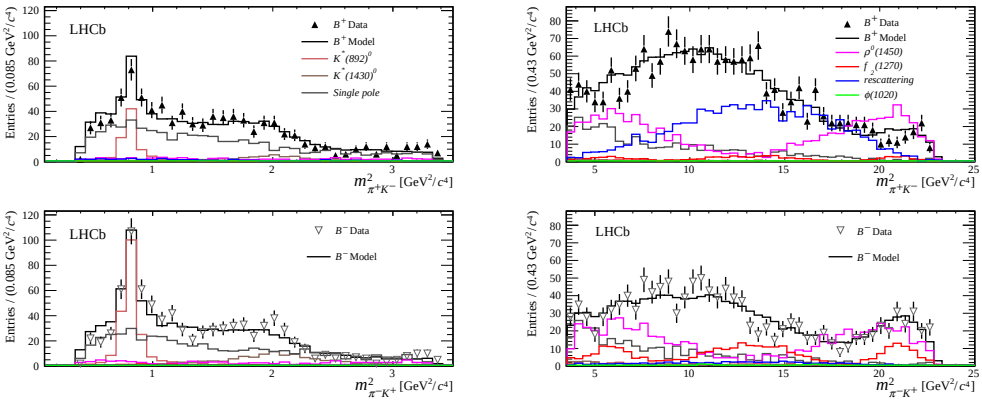


**Figure 3:** Projections of the fits to the (above) $B^+$ data and (below) $B^-$ data onto $m^2(\pi^\pm K^\mp)$ in the regions below (left) and above (right) $3.5\,\text{GeV}^2/c^4$.

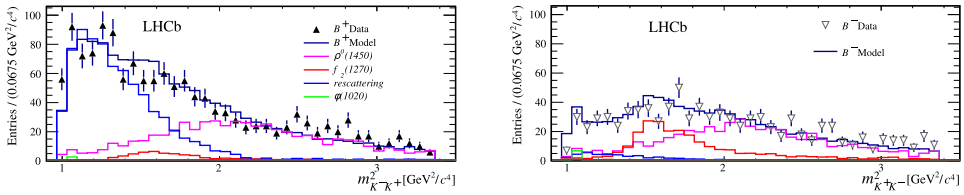


**Figure 4:** Projections of the fits to the (above) $B^+$ data and (below) $B^-$ data onto $m^2(K^+K^-)$.

Projections of the amplitude fit onto $m^2(\pi^\pm K^\mp)$ are shown in Figure 3 and onto $m^2(K^+K^-)$ in Figure 4. The flavour-averaged fit fractions and *CP* asymmetries are given in Table 2. The $m^2(\pi^\pm K^\mp)$ distributions are well described by the $K^*(892)^0$, $K_0^*(1430)^0$ and non-resonant $\pi^\pm K^\mp$ components. The single-pole non-resonant $\pi^\pm K^\mp$ amplitude is found to be the dominant contribution in the $m^2(\pi^\pm K^\mp)$ distributions. The region at high $m^2(\pi^\pm K^\mp)$ is well described by destructive interference between the $\rho(1450)^0$ and $f_2(1270)$ resonances. The $m^2(K^+K^-)$ distribution is well described by the $\phi(1020)$, $\rho(1450)^0$ and $f_2(1270)$ resonances, plus the $\pi^+\pi^- \leftrightarrow K^+K^-$ rescattering amplitude. The inclusion of the $\phi(1020)$ is found to improve the fit quality, but is not statistically significant. A large contribution from $\rho(1450)^0$ is seen in the best-fit model, which is unexpected in a $K^+K^-$ spectrum. The $\pi^+\pi^- \leftrightarrow K^+K^-$ rescattering amplitude is found to have a *CP* asymmetry of $(-66.4 \pm 3.8 \pm 1.9)\%$, which is the largest manifestation of *CP* violation observed in a single amplitude. No significant *CP* asymmetry is observed in the other amplitudes.

Systematic uncertainties in this analysis arise from mismodelling of the mass fit, the efficiency and background models, possible fit bias and the uncertainties on fixed parameters. The uncertainties on the fixed values of masses and widths of resonances are collectively found to be the largest source of systematic uncertainty. A systematic uncertainty due to the choice of amplitude model is not assigned, as the small sample size limits the scope in which alternative models can be explored.

| Contribution | Fit Fraction (%) | $\mathcal{A}^{CP}$ (%) |
|---|---|---|
| $K^*(892)^0$ | $7.5 \pm 0.6 \pm 0.5$ | $+12.3 \pm 8.7 \pm 4.5$ |
| $K_0^*(1430)^0$ | $4.5 \pm 0.7 \pm 1.2$ | $+10.4 \pm 14.9 \pm 8.8$ |
| Single pole | $32.3 \pm 1.5 \pm 4.1$ | $-10.7 \pm 5.3 \pm 3.5$ |
| $\rho(1450)^0$ | $30.7 \pm 1.2 \pm 0.9$ | $-10.9 \pm 4.4 \pm 2.4$ |
| $f_2(1270)$ | $7.5 \pm 0.8 \pm 0.7$ | $+26.7 \pm 10.2 \pm 4.8$ |
| Rescattering | $16.4 \pm 0.8 \pm 1.0$ | $-66.4 \pm 3.8 \pm 1.9$ |
| $\phi(1020)$ | $0.3 \pm 0.1 \pm 0.1$ | $+9.8 \pm 43.6 \pm 26.6$ |

**Table 2:** Fit fractions and *CP* asymmetries extracted from the $B^\pm \to \pi^\pm K^+ K^-$ amplitude fit. The first uncertainties are statistical and the second systematic.

## 4. Four-body $\Lambda_b^0$ and $\Xi_b^0$ decays

The branching fractions and triple-product asymmetries of charmless four-body $b$-baryon decays have previously been studied by LHCb in Refs. [11, 12, 13]. In Ref. [12], $3.3\sigma$ evidence for *CP* violation was measured in the T-odd triple-products of $\Lambda_b^0 \to p\pi^-\pi^+\pi^-$ decays. An analysis of *CP* asymmetries in charmless four-body $\Lambda_b^0$ and $\Xi_b^0$ decays, published in Ref. [14], is presented in these proceedings.

The six decay modes studied are $\Lambda_b^0 \to p\pi^-\pi^+\pi^-$, $\Lambda_b^0 \to pK^-\pi^+\pi^-$, $\Lambda_b^0 \to pK^-K^+\pi^-$, $\Lambda_b^0 \to pK^-K^+K^-$, $\Xi_b^0 \to pK^-\pi^+\pi^-$ and $\Xi_b^0 \to pK^-\pi^+K^-$. The three most abundant (namely $\Lambda_b^0 \to p\pi^-\pi^+\pi^-$, $\Lambda_b^0 \to pK^-\pi^+\pi^-$, and $\Lambda_b^0 \to pK^-K^+K^-$) are also studied in specific regions of phase space, corresponding to low two-body mass and those containing specific resonances, namely $a_1(1260)^+ \to \pi^+\pi^-\pi^+$, $K_1(1410)^+ \to K^+\pi^-\pi^+$, $\Delta^{++} \to p\pi^+$, $N(1520)^0 \to p\pi^+\pi^-$, $\Lambda(1520) \to pK^-$, $\rho^0 \to \pi^+\pi^-$ and $K^*(892)^0 \to K^+\pi^-$. The chosen regions of two-body invariant mass are illustrated in Figure 5. The three-body invariant mass regions are chosen to be $419 < m(\pi^+\pi^-\pi^+) < 1500\,\text{MeV}/c^2$ for the $a_1(1260)^+$ and $1200 < m(K^+\pi^-\pi^+) < 1600\,\text{MeV}/c^2$ for the $K_1(1410)^+$.

The *CP* asymmetries are determined using yields extracted from simultaneous fits to the $p\pi^-\pi^+\pi^-$, $pK^-\pi^+\pi^-$, $pK^-K^+\pi^-$, $pK^-\pi^+K^-$ and $pK^-K^+K^-$ invariant mass distributions and those of their charge-conjugate final states. The datasets are further split by years of data-taking and hardware trigger conditions. The fit models contain components for the $\Lambda_b^0/\Xi_b^0$ signal, cross-feed from $\pi$–$K$ misidentification, 4-body $B$ meson backgrounds (from $\pi$–$p$ and $K$–$p$ misidentification), partially-reconstructed 5-body $b$-hadron decays and combinatorial background. The fits for $\Lambda_b^0 \to p\pi^-\pi^+\pi^-$ are shown in Figure 6. The fits to other distributions can be found in Ref. [14].

Artificial *CP* asymmetries that arise from production and detection are cancelled using $\Lambda_b^0 \to \Lambda_c^+\pi^-$ and $\Xi_b^0 \to \Xi_c^+\pi^-$ control channels, thus the measured quantities are $\Delta\mathcal{A}^{CP} \equiv \mathcal{A}^{CP}{}_{\text{charmless}} - \mathcal{A}^{CP}{}_{\text{charm}}$. A total of 18 $\Delta\mathcal{A}^{CP}$ measurements are made in this analysis. The integrated $\Delta\mathcal{A}^{CP}$ asymmetry differences are measured to be

$$\Delta\mathcal{A}^{CP}(\Lambda_b^0 \to p\pi^-\pi^+\pi^-) = (+1.1 \pm 2.5 \pm 0.6)\,\%, \quad \Delta\mathcal{A}^{CP}(\Lambda_b^0 \to pK^-K^+K^-) = (+0.2 \pm 1.8 \pm 0.6)\,\%,$$
$$\Delta\mathcal{A}^{CP}(\Lambda_b^0 \to pK^-\pi^+\pi^-) = (+3.2 \pm 1.1 \pm 0.6)\,\%, \quad \Delta\mathcal{A}^{CP}(\Xi_b^0 \to pK^-\pi^+\pi^-) = (-17 \pm 11 \pm 1)\,\%,$$
$$\Delta\mathcal{A}^{CP}(\Lambda_b^0 \to pK^-K^+\pi^-) = (-6.9 \pm 4.9 \pm 0.8)\,\%, \quad \Delta\mathcal{A}^{CP}(\Xi_b^0 \to pK^-\pi^+K^-) = (-6.8 \pm 8.0 \pm 0.8)\,\%.$$

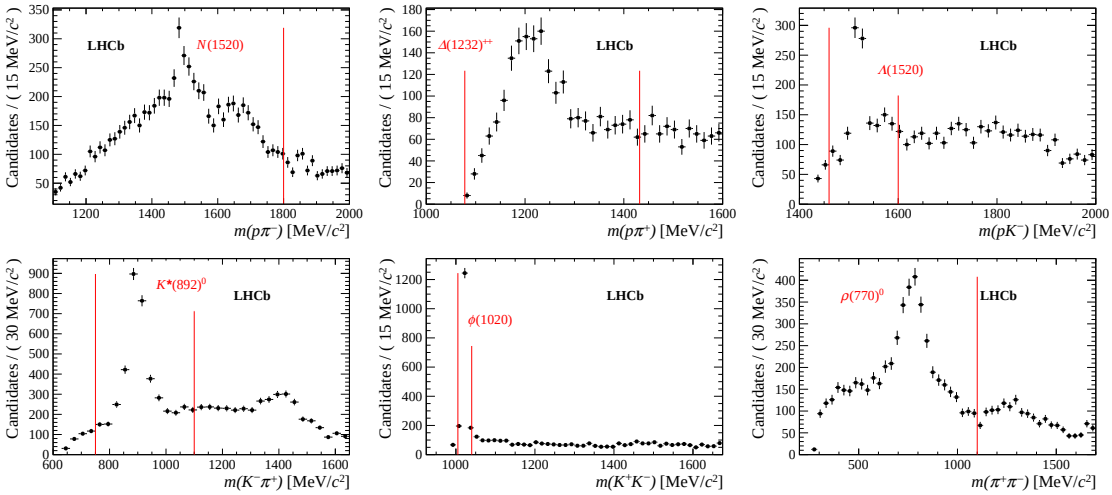


**Figure 5:** Two-body invariant mass distributions. The red lines mark the positions of cuts used to define invariant mass regions corresponding to the resonances labelled in red text. The x-axis ranges also correspond to the low two-body mass regions.

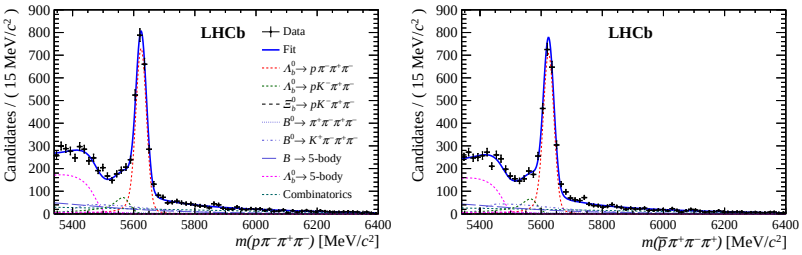


**Figure 6:** Fits to the $p\pi^-\pi^+\pi^-$ and $\overline{p}\pi^+\pi^-\pi^+$ invariant mass distributions.

The measurements of low two-body mass regions are

$$\Delta\mathscr{A}^{CP}(\Lambda_b^0 \to p\pi^-\pi^+\pi^-) = (+3.7 \pm 4.1 \pm 0.5)\,\%,$$
$$\Delta\mathscr{A}^{CP}(\Lambda_b^0 \to pK^-\pi^+\pi^-) = (+3.5 \pm 1.5 \pm 0.5)\,\%,$$
$$\Delta\mathscr{A}^{CP}(\Lambda_b^0 \to pK^-K^+K^-) = (+2.7 \pm 2.3 \pm 0.6)\,\%.$$

Finally, the measurements for the quasi-two-body decays are

$$\Delta\mathscr{A}^{CP}(\Lambda_b^0 \to pa_1(1260)^-) = (-1.5 \pm 4.2 \pm 0.6)\,\%,$$
$$\Delta\mathscr{A}^{CP}(\Lambda_b^0 \to N(1520)^0\rho^0) = (+2.0 \pm 4.9 \pm 0.4)\,\%,$$
$$\Delta\mathscr{A}^{CP}(\Lambda_b^0 \to \Delta^{++}\pi^-\pi^-) = (+0.1 \pm 3.2 \pm 0.6)\,\%,$$
$$\Delta\mathscr{A}^{CP}(\Lambda_b^0 \to pK_1(1410)^-) = (+4.7 \pm 3.5 \pm 0.8)\,\%,$$
$$\Delta\mathscr{A}^{CP}(\Lambda_b^0 \to \Lambda(1520)\rho^0) = (+0.6 \pm 6.0 \pm 0.5)\,\%,$$
$$\Delta\mathscr{A}^{CP}(\Lambda_b^0 \to N(1520)^0K^{*0}) = (+5.5 \pm 2.5 \pm 0.5)\,\%,$$
$$\Delta\mathscr{A}^{CP}(\Lambda_b^0 \to \Delta^{++}K^-\pi^-) = (+4.4 \pm 2.6 \pm 0.6)\,\%,$$
$$\Delta\mathscr{A}^{CP}(\Lambda_b^0 \to \Lambda(1520)\phi) = (+4.3 \pm 5.6 \pm 0.4)\,\%,$$
$$\Delta\mathscr{A}^{CP}(\Lambda_b^0 \to (pK^-)_{\text{high-mass}}\phi) = (-0.7 \pm 3.3 \pm 0.7)\,\%,$$

where the uncertainties are statistical and systematic. None of the measurements show significant indication of *CP* violation. Systematic uncertainties arise from the tracking and trigger efficiencies, incomplete cancellation of production asymmetries and the finite size of particle identification calibration samples.

## References


[1] LHCb collaboration, *Study of $B^0_{(s)} \to K^0_S h^+ h'^-$ decays with first observation of $B^0_s \to K^0_S K^\pm \pi^\mp$ and $B^0_s \to K^0_S \pi^+ \pi^-$*, *JHEP* **10** (2013) 143 LHCb-PAPER-2013-042, [1307.7648].

[2] LHCb collaboration, *Updated branching fraction measurements of $B^0_{(s)} \to K^0_S h^+ h'^-$ decays*, *JHEP* **11** (2017) 027 LHCb-PAPER-2017-010, [1707.01665].

[3] LHCb collaboration, *Observation of $B^0_s \to K^{*\pm} K^\mp$ and evidence of $B^0_s \to K^{*-} \pi^+$ decays*, *New J. Phys.* **16** (2014) 123001 LHCb-PAPER-2014-043, [1407.7704].

[4] LHCb collaboration, *First observation of the decay $B^0_s \to K^0_S K^*(892)^0$*, *JHEP* **01** (2016) 012 LHCb-PAPER-2015-018, [1506.08634].

[5] LHCb collaboration, *Amplitude analysis of $B^0_s \to K^0_S K^\pm \pi^\mp$ decays*, *JHEP* **06** (2019) 114 LHCb-PAPER-2018-045, [1902.07955].

[6] LASS collaboration, *A study of $K^-\pi^+$ scattering in the reaction $K^- p \to K^- \pi^+ n$ at 11 GeV/$c$*, *Nucl. Phys.* **B296** (1988) 493.

[7] LHCb collaboration, *Measurement of CP violation in the three-body phase space of charmless $B^\pm$ decays*, *Phys. Rev.* **D90** (2014) 112004 LHCb-PAPER-2014-044, [1408.5373].

[8] LHCb collaboration, *Amplitude analysis of $B^\pm \to \pi^\pm K^+ K^-$ decays*, 1905.09244 LHCb-PAPER-2018-051, [1905.09244].

[9] J. H. Alvarenga Nogueira, I. Bediaga, A. B. R. Cavalcante, T. Frederico and O. Lourenço, *CP violation: Dalitz interference, CPT, and final state interactions*, *Phys. Rev. D* **92** (2015) 054010.

[10] J. R. Pelaez and F. J. Yndurain, *The pion-pion scattering amplitude*, *Phys. Rev. D* **71** (2005) 074016.

[11] LHCb collaboration, *Measurement of branching fractions of charmless four-body $\Lambda^0_b$ and $\Xi^0_b$ decays*, *JHEP* **02** (2018) 098 LHCb-PAPER-2017-034, [1711.05490].

[12] LHCb collaboration, *Measurement of matter-antimatter differences in beauty baryon decays*, *Nature Physics* **13** (2017) 391 LHCb-PAPER-2016-030, [1609.05216].

[13] LHCb collaboration, *Search for CP violation using triple product asymmetries in $\Lambda^0_b \to pK^-\pi^+\pi^-$, $\Lambda^0_b \to pK^-K^+K^-$, and $\Xi^0_b \to pK^-K^-\pi^+$ decays*, *JHEP* **08** (2018) 039 LHCb-PAPER-2018-001, [1805.03941].

[14] LHCb collaboration, *Measurement of $\Delta\mathscr{A}^{CP}$ in charmless four-body $\Lambda^0_b$ and $\Xi^0_b$ decays*, 1903.06792 LHCb-PAPER-2018-044, [1903.06792].


PoS(EPS-HEP2019)215